Heliyon 10 (2024) e29913

Contents lists available at ScienceDirect

Heliyon

journal homepage: www.cell.com/heliyon

Research article

CerviLearnNet: Advancing cervical cancer diagnosis with reinforcement learning-enhanced convolutional networks

Shakhnoza Muksimova, Sabina Umirzakova *, Seokwhan Kang, Young Im Cho **

Department of Computer Engineering, Gachon University, Sujeong-gu, Seongnam-si 461-701, Gyeonggi-do, South Korea

ARTICLE INFO

Keywords:
Reinforcement learning
Cervical cancer
Machine learning
Classification
Deep learning
Artificial intelligence

ABSTRACT

Women tend to face many problems throughout their lives; cervical cancer is one of the most dangerous diseases that they can face, and it has many negative consequences. Regular screening and treatment of precancerous lesions play a vital role in the fight against cervical cancer. It is becoming increasingly common in medical practice to predict the early stages of serious illnesses, such as heart attacks, kidney failure, and cancer, using machine learning-based techniques. To overcome these obstacles, we propose the use of auxiliary modules and a special residual block, to record contextual interactions between object classes and to support the object reference strategy. Unlike the latest state-of-the-art classification method, we create a new architecture called the Reinforcement Learning Cancer Network, "RL-CancerNet", which diagnoses cervical cancer with incredible accuracy. We trained and tested our method on two well-known publicly available datasets, SipaKMeD and Herlev, to assess it and enable comparisons with earlier methods. Cervical cancer images were labeled in this dataset; therefore, they had to be marked manually. Our study shows that, compared to previous approaches for the assignment of classifying cervical cancer as an early cellular change, the proposed approach generates a more reliable and stable image derived from images of datasets of vastly different sizes, indicating that it will be effective for other datasets.

1. Introduction

Cervical cancer is the fourth most frequent type of cancer in females and is responsible for the deaths of many women worldwide every year. In 2020, the World Health Organization (WHO) reported 604,127 new cases of cervical cancer in women and 341,831 deaths related to cervical cancer [1]. According to the WHO, cervical cancer boasts the highest rate of successful treatment compared to other forms of cancer. Identifying cervical cancer at an early stage continues to be the most significant challenge in the fight against this disease. To prevent cervical cancer in women, screenings are conducted, and precancerous lesions are treated. However, most women in impoverished nations are at risk of a problematic cancer process because they lack adequate medical facilities, a shortage of specialists, and costly screening methods. Computer-assisted decision support systems play a crucial role in finding solutions to these problems.

In recent years, there has been an increase in interest in developing computer-aided diagnosis (CADx) systems for cervical cancer screening, which is directly tied to the prevalent practical issues observed in these under-resourced health institutions, including a

* Corresponding author.
** Corresponding author.
E-mail addresses: sabinatuit@gachon.ac.kr (S. Umirzakova), yicho@gachon.ac.kr (Y.I. Cho).

https://doi.org/10.1016/j.heliyon.2024.e29913
Received 3 December 2023; Received in revised form 16 April 2024; Accepted 17 April 2024
Available online 24 April 2024

shortage of specialist personnel and equipment. Manual microscopic inspection of cervical cytology smears is an arduous and time-consuming job that simultaneously requires a great amount of skill from a cytotechnologist. Computer vision (CV) and machine learning (ML) are two methodologies that are often employed in CADx systems to reduce the dependency on the manual microscopic examination of cytology smears. In recent years, automated decision-making systems have become more common in the medical industry. In the last ten years, several publications have become available on diagnosis based on ML, most notably for cancer. Examples of cancers that are subject to computer-assisted diagnosis include lung cancer [2], gastric cancer [3], prostate cancer [4,5], pancreatic cancer [6,7], and breast cancer [8–11].

Recent studies by scientists have mostly focused on improving the precision of classification tasks, particularly regarding massive datasets and sophisticated approaches. The performance of conventional approaches is good when used on relatively small datasets; however, the results are unsatisfactory when applied to much larger datasets. The convolutional neural network (CNN) has previously been used as a technology that saves lives when working with extensive collections of images. According to authors [12,13], the CNN can achieve extraordinarily high classification accuracies in various applications. This accomplishment is due to its capacity to learn, which is made possible by its intricate architecture. When trained CNNs are applied to the challenge of large-scale object identification, image processing becomes much simpler. The data that the CNN has learned may be applied to various datasets to address other issues. CNNs that have been pretrained on object identification are typically chosen by those working in the CV field for use in ad hoc feature representation for tasks related to the processing of visual input [14].

The novel aspect of this study is that it uses a revised version of the EfficientNetV2 model to detect cervical cancer. The following is a description of the most important contributions and innovations of our research in this study.

- To automate the process of cancer categorization, we propose a novel framework that combines CNNs with a reinforcement learning algorithm.
- We use a general technique to train the classifier in conjunction with a supervised learning agent, also known as the deep Q_m network.
- Supporter modules are unique residual blocks that we propose for capturing contextual interactions between object classes to aid in the refer-by-object approach.
- We build a unique architecture called Reinforcement Learning Cancer Network (“RL-CancerNet”) that diagnoses cervical cancer more accurately than the most current state-of-the-art (SOTA) classification methods.

The remainder of this paper is organized as follows. An overview of previous research is presented in Section 2. The proposed method is described in section 3. The dataset, experimental results, and discussion are presented in Section 4. Finally, the conclusions of the study and future directions are presented in Section 5.

2. Research current analysis

Deep learning has made significant strides in enhancing the accuracy of various applications [15]. This technology, known for its remarkable precision across numerous domains, has emerged as the forefront of machine learning advancements. Deep learning and Convolutional Neural Networks (CNNs) have found successful applications in tasks like detecting breast cancer [16], recognizing skin cancer [17], and analyzing COVID-19 [18]. Notably, many studies rely on CNNs, which have been the go-to standard for classifying and segmenting 3D medical images. However, these networks have inherent limitations in capturing long-range relationships [19].

To address these limitations, the transformer architecture was introduced Since the end of 2020, there has been a growing interest in research involving transformers. In some areas, transformer-based research has now outperformed research based on CNNs in tasks such as image classification, object detection, and image segmentation [20]. Notably [21], were pioneers in proposing a vision transformer for image classification. They introduced a novel approach that doesn’t focus on individual pixels but instead concentrates on small sections of an image. They believe that there is no need to rely on CNNs, and that utilizing direct, pure transformers based on sequences of image patches can effectively handle image classification tasks [22]. introduces CerviFormer, a new model for classifying Pap smear images using cross-attention and latent Transformer techniques. It efficiently handles large, high-dimensional image data and achieves high accuracy. However, it does not yet consider confounding factors like menstrual cycle and age, which are identified as areas for future improvement. The CerviFormer avoids applying conventional QKV self-attention directly to the input data array, opting instead for cross-attention on the input and latent array before feeding it to the Transformer block.

Artificial intelligence (AI) and deep learning have assumed a crucial role in various aspects of medical science, including the classification of cells, medical image analysis, and data generation and interpretation [23]. As these technologies continue to evolve, they have become more cost-effective and time-efficient than traditional methods like Pap smears, colposcopy, and cervicography [24]. Importantly, AI-driven approaches are not influenced by human subjectivity. Although they cannot replace the expertise of gynecologists in pathological evaluations, they significantly assist in clinical diagnosis, enhancing diagnostic efficiency and reducing the subjective aspects of diagnosis.

Numerous studies have addressed the classification and detection of cervical cancer. CNNs [25] have been proposed to automatically acquire multi-level features through deep hierarchical structures. For example [26], study investigates automated techniques for early cervical cancer detection using deep learning. It compares two approaches: utilizing pre-trained models as feature extractors with machine learning classifiers and applying transfer learning with pre-trained models for direct image classification. In the article [27] presents an approach to cervical cancer detection by integrating deep learning architectures with machine learning classifiers and a fuzzy min-max neural network. It focuses on the accurate classification of Pap-smear images, using pre-trained models like Alexnet,

ResNet-18, ResNet-50, and GoogleNet [28]. explores the use of Deep Learning and Genetic Algorithms for classifying cervical pre-cancerous cells, a crucial but challenging task due to the limited availability of data. It leverages pre-trained CNN, specifically GoogLeNet and ResNet-18, for feature extraction from limited datasets. These features are then optimized using a Genetic Algorithm for feature selection and classified with Support Vector Machines [29]. introduces an advanced deep-learning model that enhances the accuracy of cervical cell smear image analysis by integrating an improved Faster R–CNN, shallow feature enhancement networks, and generative adversarial networks. The model aims to tackle the complexity of pathological images by enhancing data feature transformation, improving the localization of weak cells, and boosting detection capabilities through data augmentation [30]. introduces an approach for cervical cell classification combining transfer learning and knowledge distillation, aimed at overcoming issues of parameter redundancy and poor model generalization. It utilizes transfer learning for feature sharing across domains and knowledge distillation for model-to-model learning, incorporating a multi-exit classification network with a global context module in each branch for enhanced contextual understanding. A self-distillation technique helps shallow classifiers learn from deep ones, improving generalization through averaged classifier outputs [31]. addresses cervical cytology image classification by exploring the integration of local and global features using a novel Deep Integrated Feature Fusion (DIFF) block. This approach combines features from both CNN and visual transformer branches to enhance image classification. Additionally, they explored [32] the attention mechanism and proposed an innovative end-to-end attention recurrent convolutional network (ARCNet) for scene classification, making noteworthy contributions to the field of image classification [33]. presented a CNN for classifying cervical cells in Pap smear images, achieving 91.13 % accuracy. It used segmented and augmented images from the SIPaKMeD dataset, emphasizing its potential for early cervical cancer detection. The primary limitation of the method is related to the size of the dataset used for training. The model needs to be trained on a larger pool of Pap smear images to achieve better generalization. This implies that the current dataset may not be diverse or extensive enough to ensure that the model can accurately classify a wide range of cervical cell types encountered in different populations or under varying conditions [34]. introduces a Mask Region-Based Convolutional Neural Network (RCNN) for diagnosing cervical cancer using Pap smear images. It achieves over 60 % mean Average Precision and 70 % F1-scores for cell categorization. The method uses labeled samples from medical consultants and datasets like SIPaKMeD and Mendeley. Its main feature is generating automatic reports to help medical professionals quickly identify malignant cells in the images. One of the main limitations of the method is the challenge posed by overlapping cells in Pap smear images. This overlap makes it difficult for deep learning algorithms to accurately distinguish, classify, and detect different types of carcinogenic cells. Additionally, the use of different color schemes in different laboratories further complicates the application of uniform diagnostic and detection tools across various settings.

However, it is worth noting that while the neural network framework based on CNNs has demonstrated good accuracy in the classification of cervical cancer smear cell images, it demands substantial computational resources, and the network depth needs to reach a certain level to capture intricate image details. In contrast, transformers offer advantages, as the number of operations required for calculating associations between positions remains consistent regardless of their distance, thanks to self-attention mechanisms, making them a promising alternative in this context.

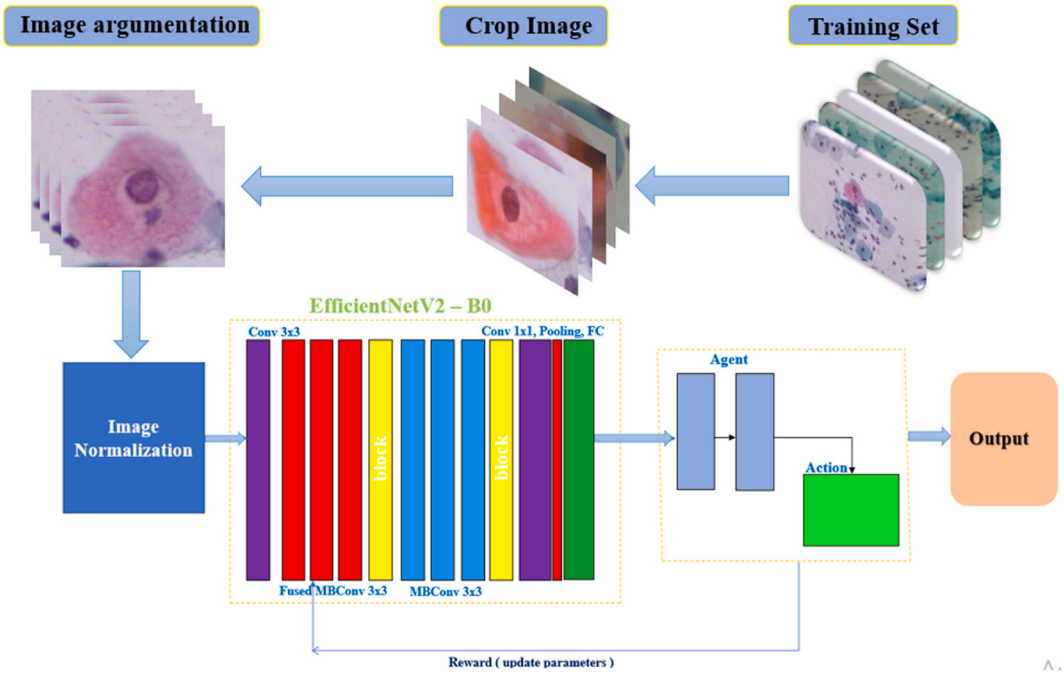

Fig. 1. Overview of the workflow of the proposed method.

3. Proposed method

This section contains a description of the methods used in this study. For a model to be well-fitted using deep learning, it is necessary to have a significant quantity of labeled data. Nevertheless, many datasets are already publicly available, expanding the application of deep learning into the areas of these open-access datasets. As deep-learning algorithms continue to find new uses, there is an increased need for data in these uncharted fields. By focusing only on the data points that assist in the building of a powerful model for the job, the active learning method provided here offers a potential solution to the problem of too much data and insufficient time to interpret it. It is recommended that active learning workflow be framed as a reinforcement learning issue. This framework is used for medical image classification, as shown in Fig. 1, and many experiments are carried out. A CNN is used to produce seed weights, which are then used in the implementation of the model. The representative then gathers a sample at each stage and assigns a category. The agent receives a reward from the environment for each act of categorization, and the reward that the minority class receives is higher than the reward that the majority class receives. The agent will, in the end, discover the best course of action to take with the assistance of a specific reward function and a conducive learning environment.

The minor role of RL stems from the inherent complexities and challenges associated with learning from environmental feedback, especially when juxtaposed with the direct, pattern-recognition abilities of CNNs. RL learning process can be slow and requires a lot of data to achieve significant performance, which contrasts with the often more immediate and tangible benefits observed with CNNs in perception tasks. Integrating CNNs with RL involves more than just combining their functionalities it requires a thoughtful approach to leverage the perceptual capabilities of CNNs to inform and enhance the decision-making process of RL. This integration aims to create a system where perception and action are seamlessly connected, allowing for sophisticated interactions with the environment that are both informed and adaptive. However, this combination also introduces complexity. It requires careful tuning and coordination between the CNN and RL components to ensure that the system can learn effectively and efficiently. The challenges include ensuring the RL component can act on the high-level features extracted by the CNN, managing the computational demands of training both components, and dealing with the potentially sparse or delayed rewards that are common in RL settings. While the RL component may initially seem to play a supporting role to the more immediately impactful CNNs within the framework, its contribution to the overall system's ability to make informed and adaptive decisions in complex environments is crucial. The integration of CNNs and RL represents a promising area of research that could lead to significant advancements in AI capabilities, provided the challenges inherent in such a synthesis can be effectively addressed.

3.1. Baseline EfficientNetV2

The EfficientNetV2 model is proposed for cervical cancer diagnosis. To improve the model's picture recognition rate when presented with complex backgrounds where the cervical cancer information is not noteworthy, we include the r-by-object supporter block in the Fused MBConv and MBConv structures to weight the topic information so that the major feature information may be learned during the network training process. During this time, a supporter block structure should be added to the network structure to increase the effectiveness of the model, and to increase the stability of the model while it is being trained. The enhanced RLCancerNet demonstrates a gain of 0.79 %, bringing the total recognition accuracy to 99.32 %. This is in comparison with EfficientNetV2, which achieves 98.53 %.

3.2. Supporter block

Fig. 2 depicts the Supporter Block consisting of architecture levels responsible for deriving contextual relations from features: the convolution layer and the bidirectional long short-term memory (BiLSTM) layers as a one-shot attention mechanism. More precisely, when the global pooling of modules collects global spatial information, the block distributes more embedded high-level contextual information across broad neighborhoods in each feature map. In contrast, the BiLSTM layers distribute spatial correlations throughout

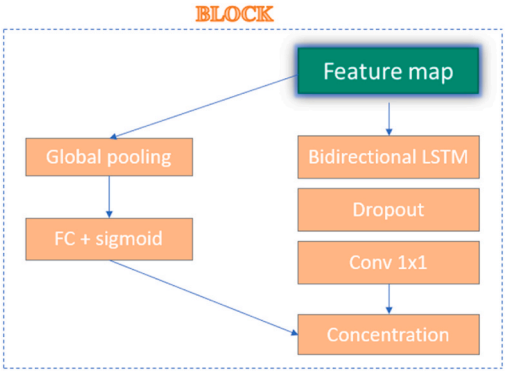

Fig. 2. Blocks for Rethinker are designed under a layer of Conv3D and convLSTM.

the image patches and store low-level contextual information across local neighborhood pieces of fractured feature maps. The primary branch comprises either an attention-based BiLSTM block or a bidirectional long short-term memory that can store information in both directions. BiLSTM is a version of LSTM that trains two LSTMs instead of one and can access the long-range context in time series data in both the forward and backward directions. This makes it suitable for analyzing incentives from RL. The BiLSTM block is given a feature map, followed by the transpose of the temporal dimension of the time series and dropout to prevent overfitting. Ultimately, the outputs of the two branches are concatenated and fed into a subsequent network layer. To enhance the model ability to recognize images amidst complex backgrounds where cervical cancer indicators may not be prominent, a novel approach has been introduced. This approach involves integrating a supporter block within the Fused MBConv and MBConv frameworks. The purpose of this supporter block is to emphasize subject information, thereby allowing the model to learn significant feature information more effectively during training. This enhancement, referred to as RLCancerNet, has led to an improvement in recognition accuracy by 0.79 %, reaching a total accuracy of 99.32 %. This is a notable improvement compared to the original EfficientNetV2 model, which achieved an accuracy of 98.53 %. The supporter block is depicted as being composed of various architectural levels that are tasked with deriving contextual relationships from features. This includes a convolution layer and BiLSTM layers, which together function as a one-shot attention mechanism. Specifically, the block distributes more embedded high-level contextual information throughout the feature map while also handling spatial correlations and low-level contextual information across local neighborhoods. The BiLSTM layers, which store information in both forward and backward directions, are particularly highlighted for their ability to analyze data sequences effectively. This is further augmented with dropout techniques to prevent overfitting. The combined output of these processes is then fed into subsequent layers of the network, enhancing the model overall performance and stability during training.

The result of the BiLSTM algorithm is an $F_s \in R^{H\times W\times D}$ map that goes through the convolutional 1×1 layer, $F_s^{'} \epsilon R^{H\times W\times D}$, and then returns to the residual blocks. The following is an explanation of how the block operation works.

$$F_s^{'} = L_{fi}\left(\left[\Phi\left(L_{fi}(F_s, M)|F_s, M\right)\left|L_{fi}r_t\right|c_t\right], M\right) \tag{1}$$

where L_{fi} is the future map layer, L_{fi}: $R^{H\times W\times C}\rightarrow R^{N^2\times H^{'}\times W^{'}\times D}$ offers local spatiotemporal data, and $r_t = L_{fi}(F_s,M)$. In practice, feature maps are converted into patches across channels, which are then used as spatiotemporal data. It is presumed that anything with a patch size of H′W′ (where H′ = H/N and W′ = W/N) is either a single item or a collection of objects in Equation (1). The value of N indicates the dimensional slicing coefficient that applies across the width and height of the feature map.

Therefore, Φ, the BiLSTM Φ - algorithm, should be implemented using $R^{N^2\times H^{'}\times W^{'}\times D}\rightarrow R^{N^2\times H^{'}\times W^{'}\times D}$ while maintaining the depth of the feature map. By examining patches, objects, or groups of items in sequential order, BiLSTM can encode spatiotemporal correlations between the characteristics. The results of this process are then passed on as spatiotemporal data.

The learning strategy is known as reinforcement Active Learning for Image Classification: A Method for In-Depth Reinforcement Learning, Called RLCancerNet: A Reinforcement Learning-Based population weight pretraining algorithm is integrated with reinforcement learning for cervical cancer. The three major reinforcement learning components are state, action, and reward. In RL, an agent is charged with learning to perform a particular action in a specific situation. This is a part of the learning process. The RL agent becomes eligible for a reward after the assignment they are working on is completed. During their employment, the objective of the RL agent is to assemble the most significant number of awards. In the next section, we describe each of the three aspects that constitute our framework. Next, we provide an overview of this framework.

1. Declare that the RL agent will assess the circumstances at each stage of the procedure and decide which course of action is appropriate in response to those circumstances. If the state wants the RL agent to make better-informed choices, it is responsible for providing them with all the pertinent information. A continuous vector s created by combining the attributes recovered by the CNN model with the prediction scores of the labeled samples. This vector is then used to describe the state. The state space can be described using the notation $P = \{pf\}$, where pf $= x_i^t, f(X_i^t)$ and superscript t stands for the system's current state at a given time t. This notation can be used to mathematically express the state space.
2. This action is performed to predict the label text. Because the classification presented consists of three classes, at $\in \{\ \}$ 0, 1, 2, the number zero indicates the minority class, the number one represents the precancer class, and the number two represents the majority class.
3. Reward (Rt): The concept of reward considers the completion of an activity. If an agent has the appropriate categorization, the reward they receive is positive; otherwise, the reward they receive is negative. It is unacceptable for this incentive to be the same across courses. Because the amount of reward and action is meticulously tuned, rewards can significantly increase the model performance. In this particular piece of work, the award for action is determined using the following Equation (2):

$$R_t(s_t, a_t, n_t) = \begin{cases} \{+1, a_t = y_t \text{ and } s_t \epsilon M_n, \\ -1, a_t \neq y_t \text{ and } s_t \epsilon M_n, \\ \partial, a_t = y_t \text{ and } s_t \epsilon M_c, \\ -\partial, a_t \neq y_t \text{ and } s_t \epsilon M_c. \end{cases} \tag{2}$$

where M_n and M_c represent the minority and majority classes, which are normal, precancer, and cancer, respectively, and where ∂ is a number that falls somewhere in the range [0,1]. As a result of having fewer data, the minority class becomes more crucial, which causes the reward ∂ to become smaller than 1/-1. To make the minority class more comparable to the majority class, we could, in effect, provide greater weight to members of the minority class. The significance of the value ∂ becomes apparent when we look at the

findings.

In the field of reinforcement learning, the goal is to achieve a high limit for the following expression by maximizing the discounted cumulative reward or, in other words, to maximize the maximum possible value for the following expression:

$$d_t = \sum_{m=0}^{\infty} \gamma^m. \tag{3}$$

The value of all collected return points from the agent's searches in space is included in Equation (3), which is referred to as the return function, and is the discount factor, c ∈ (0, 1,2] [35] is the effect factor of each reward. The quality of a state-action combination is measured by the function, Q_m:

$$Q_m^{\pi}(s,a) = I_{\pi}[d_t | s_t = s, a_t = a]. \tag{4}$$

The following is an expansion of Equation (4), based on Bellman's formula:

$$Q_m^{\pi}(s,a) = I_{\pi}\left[R_t + \gamma Q_m^{\pi}(s_{t+1}, a_{t+1}) \middle| s_t = s, a_t = a\right]. \tag{5}$$

More cumulative rewards may be obtained if the supported function Q_m is optimized to its full potential. The optimal strategy of π* is evaluated by taking into consideration the function Q_m^* in the following way:

$$\pi^*(a,s) = \begin{cases} 1, a = argmax_a Q_m^*(s,a), \\ 0, else \end{cases} \tag{6}$$

When Equations (5) and (6) are combined, the function Q_m^* may be represented as follows:

$$Q_m^*(a|s) = I_{\pi}\left[R_t + \gamma\, max_a Q_m^*(s_{t+1}, a_{t+1}) \middle| s_t = s, a_t = a\right]. \tag{7}$$

In a state of space with a low number of dimensions, function Q_m can be readily solved by using a table. However, the table method is insufficient when many spaces are combined. Q-learning techniques have been used to find a solution to this issue. The tuple (s, a, r, s0) obtained from Equation (7) and preserved in these algorithms is referred to as the experience replay memory M. The agent obtains a mini-batch B from M and applies the gradient descent algorithm to these data following Equation (8), which is presented below:

$$G(\theta)_k = \sum_{(s,a,r,s') \epsilon B} (y - Q_m(s,a;\theta_k))^2 \tag{8}$$

where 'y' represents a guess as to the value of the function Q_m, which is written down as follows:

$$y = \begin{cases} r, end = True, \\ r + \gamma\, max_{a'} Q_m(s' a' \theta_{k-1}), else, \end{cases} \tag{9}$$

where in Equation (9) s′ is the next s state, a′ is the action carried out in s, and end refers to whether or not the agent makes an incorrect categorization of the minority class. Finally, the policy weights can be modified as follows:

$$\theta = \theta + l \frac{\nabla L(\theta_k)}{\nabla(\theta_k)}, \frac{\nabla L(\theta_k)}{\nabla(\theta_k)} = -2 \sum_{(s,a,r,s') \epsilon B} (y - Q_m(s,a;\theta_k)) \frac{\nabla Q_m(s,a;\theta_k)}{\nabla(\theta_k)} \tag{10}$$

In conclusion, it is possible to obtain the optimum function Q_m^* by reducing the loss function, as shown in Equation (10). Notably, Q_m is used to determine the optimal strategy for π*, which is significant because Q_m^* is the best model for the proposed classifier.

Algorithm 1: Cervical Cancer Classification with Meta-Learning Ensemble CNN

1: Input: Labeled cervical cancer image dataset;
2: Output: Classified images as benign or malignant;
3: Preprocess the dataset to normalize and augment the images;
4: Initialize the RL-CancerNet meta-model with auxiliary modules;
5: for number of training epochs do
6: Sample batch of n images {I1, I2, …, In} from the dataset D;
7: Feed In through the meta-model to obtain preliminary classification results;
8: for each auxiliary module in the meta-model do
9: Leverage the module to capture contextual interactions between cell classes;
10: end for
11: Incorporate the special residual block to enhance feature extraction;
12: for each classification result do
13: Compare the prediction with the actual label to assess accuracy;
14: end for
15: Generate classification output Iclassifiedn;
16: Calculate loss between Iclassifiedn and the true labels;
17: Update model weights using backpropagation and an optimization algorithm;

(*continued on next page*)

(*continued*)

18: Monitor and record the learning curves for accuracy and loss;
19: end for
20: After training, test the model on a separate set of images;
21: Fine-tune the model based on test results if necessary;
22: Deploy the trained model for real-world cervical cancer screening and diagnosis.

(*continued on next page*)

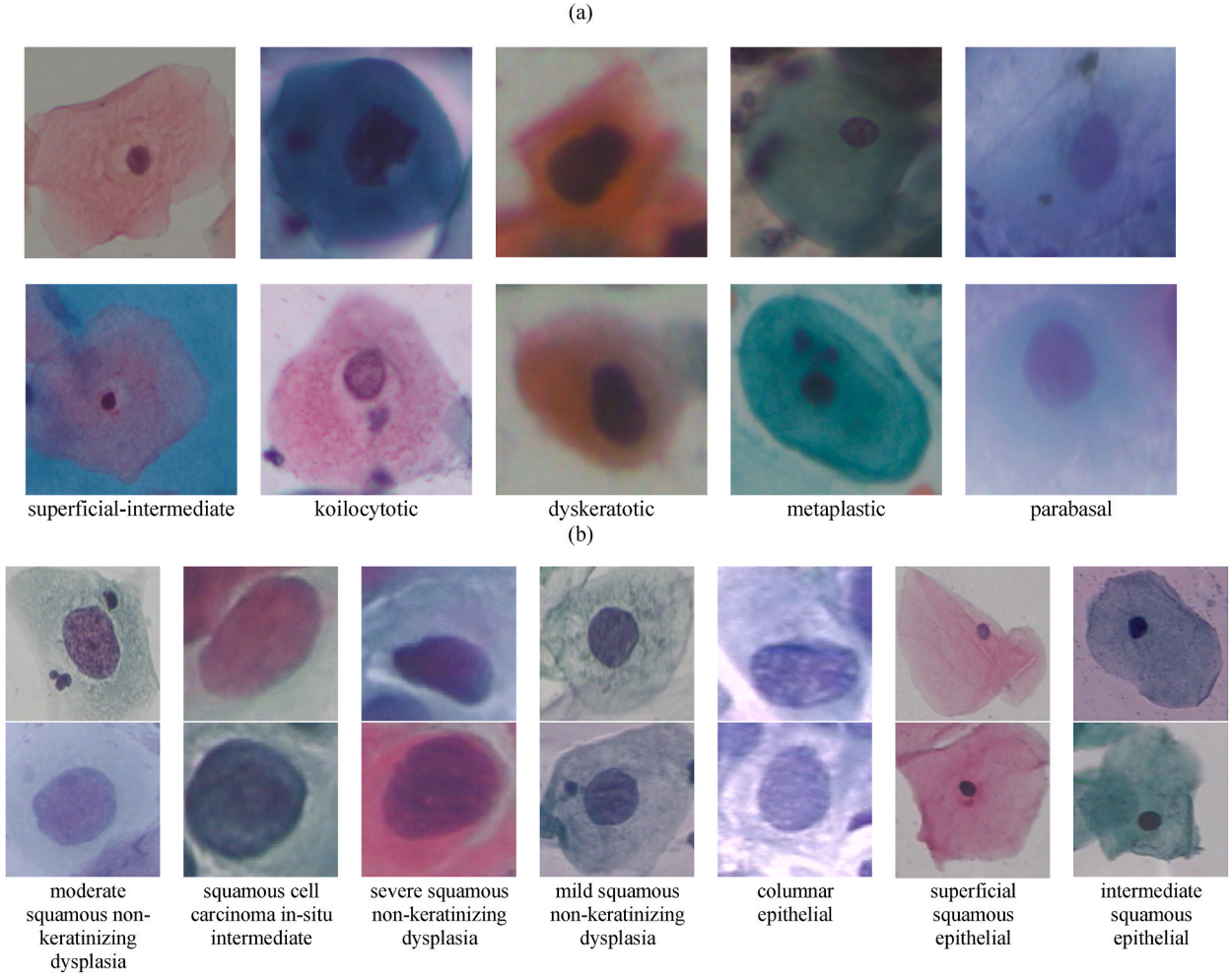

Fig. 3. Description of cervical cancer datasets: a) SipaKMed, and b) Herlev.

(*continued*)

4. Description of the dataset and metric

4.1. Implementation details

Our training setup was based on the PyTorch framework [36], and the model was trained using the following configuration. The generator network was optimized using the Adam optimizer [37]. We performed experiments on a device using an NVIDIA GeForce RTX 3080 Ti GPU. The test equipment was implemented using an Intel® Core™ i7-11700K 3.60 GHz central processing unit (CPU). The software specifications of the test environment were CUDA 11.1, cuDNN 8.1.1, and Python 3.8..

4.2. Dataset and augmentation

In this study, we use two public cervical cytology datasets to evaluate the proposed classification model..

1) The SipaKMeD Pap Smear dataset [38] consists of 4049 isolated cell images (extracted from 966 complete slide images) that are divided into five groups based on cytomorphological features; details are presented in Table 1 and Fig. 3 (a).
2) The Herlev Pap Smear dataset [39] contains 917 single-cell images unevenly distributed among seven different classes and is available to the public; details are presented in Table 2 and Fig. 3 (b).

For the SipaKMeD and Herlev datasets, which contain 4049 and 917 images respectively, we implemented a variety of augmentation techniques to simulate a broader range of real-world conditions. These techniques included: Images were rotated at various angles to simulate different orientations of cervical cells. Horizontal and vertical flipping were applied to mirror the images, representing a wider array of cell positions. Random zooming in and out of images helped the model to learn from different scales of cell structures. Shifting the images horizontally and vertically introduced variability in the cell positioning within the image frame. Applying shear transformations simulated a range of perspectives, aiding in the recognition of cells from different viewpoints. Variations in brightness and contrast settings helped to mimic different lighting conditions encountered in clinical settings. By augmenting our datasets, we effectively increased the variability and complexity of the training data, which is crucial for developing a robust model capable of generalizing well to unseen data. This strategy allowed RL-CancerNet to learn from an enriched set of images that better represent the diverse conditions encountered in real-world diagnostic scenarios. Data augmentation not only addressed the limitations posed by the small dataset sizes but also contributed to the model's improved accuracy and generalizability. It is a testament to our commitment to overcoming dataset constraints and enhancing the reliability of RL-CancerNet for cervical cancer diagnosis..

4.3. Metrics

Six conventional performance measures were employed to assess the classification performance of the proposed model. These metrics are called accuracy, recall, precision, F-measure, and G-means [40], and their definitions according to Equation (11):

$$Accuracy = \frac{TP + TN}{TP + TN + FP + FN},$$

$$Recall = \frac{TP}{TP + FN},$$

$$Precision = \frac{TP}{TP + FP}, \tag{11}$$

Table 1
Distribution of information in the SipaKMed dataset.

Category name	Quantity	Property
Superficial-intermediate	813	Normal
Koilocytotic	825	Abnormal
Dyskeratotic	813	
Metaplastic	793	Bening
Parabasal	787	
Total number of images	4049	

Table 2
Distribution of information in the Herlev dataset.

Category name	Quantity	Property
Moderate squamous non-keratinizing dysplasia	146	Abnormal
Squamous cell carcinoma in-situ intermediate	150	
Severe squamous non-keratinizing dysplasia	197	
Mild squamous non-keratinizing dysplasia	182	
columnar epithelial	98	Normal
superficial squamous epithelial	74	
intermediate squamous epithelial	70	
Total number of images	917	

$$F_{measure} = \frac{2 \times Recall \times Precision}{Recall \times Precision}$$

$$Specificity = \frac{TN}{TN + FP},$$

$$G - means = \sqrt{Recall \times Specificity}$$

where the number of accurately classified positive records is shown by the term (TP)-True Positive, (TN)-True Negative, (FN)-False Negative, and (FP)-False Positive. The F-measure and G-means algorithms are two methods often used to analyze unbalanced classifications [41], and they correspond well with the sample distribution of our dataset and the rationale for the existence of our suggested technique. It is also important to note that our assessment was based on each photograph. The intelligent myocarditis categorization system can filter full examinations and highlight particular pictures for closer examination by physicians using this method. For this particular objective, measures with a low FP and a high recall are preferable.

5. Experimental results

In our investigation, we propose a meta-learning ensemble method utilizing CNNs aimed at enhancing the diagnostic accuracy and dependability for cervical cancer. The precise classification of cancer stages is crucial, and our meta-model stands out, especially in distinguishing benign from malignant cases. Implementations of data augmentation and dropout regularization have markedly bolstered our model robustness.

To ensure the reliability and validity of our findings, we employed a rigorous k-fold cross-validation strategy with k set to 5 (5-CV). This approach allowed us to maximize the use of our dataset by systematically rotating the training and testing subsets, thereby ensuring that every data point contributed to the model training and validation. This method not only provided a robust estimate of RL-CancerNet performance but also allowed for a comprehensive statistical analysis of the model's diagnostic capabilities, including metrics such as accuracy, precision, recall, and the F-1 score, accompanied by their respective mean, standard deviation, median, minimum, and maximum values. These methodological choices reflect our commitment to developing a robust and reliable diagnostic tool for cervical cancer, grounded in a thorough and thoughtful approach to model training and validation. Through the strategic application of data augmentation, a weighted loss function, and k-fold cross-validation, we aimed to present a model not just of technical excellence but of significant clinical relevance and utility. To improve upon our methodology and address this critical point, we incorporate testing on independent datasets that were not used in any phase of the model's training or internal validation. This step will ensure a more rigorous assessment of the model's performance and its applicability to diverse real-world conditions. By comparing the model performance on these independent test sets with the results obtained from the initial datasets (SipaKMeD and Herlev), we aim to provide a clearer picture of its generalizability across different populations and imaging conditions. (new Table)Our hybrid model based on the RL model demonstrated remarkable improvements applied to the cancer detection task for both the SipaKMeD med and Herlev Pap Smear datasets. As can be seen from the data given in Table 1, we tested the experience with various well-known classification models, such as ResNet50, Xception, EfficientNetV1, VGG 16, MobileNet V2, and Inception V2, all of which produced results that were lower than that of the proposed model on accuracy 1 % and 1.2 %.

Table 3 presents a comparison of classification performance metrics across various deep learning models, including ResNet50, Xception, EfficientNetV1, VGG16, MobileNetV2, Inception V2, and a Proposed Method. These metrics are indicators of how accurately

Table 3
Comparison of classification performance using different models.

Metric	ResNet50 [42]	Xcepsion [43]	EfficientNetV1 [44]	VGG 16 [45]	MobileNetV2 [46]	Inception V2 [47]	Proposed Method
Accuracy	98.52	96.16	97.41	96.23	97.55	98.28	**99.70**
Precision	97.31	98.15	96.16	95.12	96.99	98.14	**99.36**
Recall	98.38	99.21	95.63	95.60	97.82	98.9	**99.90**
F1	97.70	98.36	95.47	95.28	97.25	98.70	**99.72**

and reliably each model can classify data into categories. The Proposed Method showcases superior performance across all metrics compared to the established models. Specifically, it demonstrates the highest accuracy (99.70 %), precision (99.36 %), recall (99.90 %), and F1 score (99.72 %). These metrics suggest that the Proposed Method not only correctly classifies a high percentage of accuracy but also maintains a balance between precision and recall—minimizing both false positives and false negatives.

In contrast, the other models show varying degrees of performance. While some like Xception and Inception V2 exhibit high recall, indicating they are good at identifying relevant instances, their precision scores are lower, hinting at a higher rate of false positives. The precision and recall trade-off is crucial in classification tasks, as it impacts the model applicability to real-world scenarios Fig. 4. High precision models are preferable in situations where false positives are costlier, while high recall models are ideal when missing a positive instance has greater consequences. The F1 score, a harmonic mean of precision and recall, shows that while models like Xception and ResNet50 have commendable performance, they still lag behind the Proposed Method. Additionally, we have closely tracked the learning curves for all evaluated models, observing consistent improvements in training alongside a steady decline in validation losses. Initially, our model was trained on the SipaKMeD and Herlev datasets, which include both benign and malignant classes. Further testing on cervical cancer cell images resulted in significant accuracy gains within just 60 training epochs. Our meta-model also demonstrated a more efficient convergence of training and validation losses compared to standard CNN models, suggesting its potential applicability to other datasets in the medical domain.

This suggests that the Proposed Method is better at maintaining a balance between identifying relevant instances and minimizing incorrect classifications.

1. A cutting-edge solution for the automation-assisted reading of cervical cancer based on convolutional neural networks.
2. An ensemble of CNN models for the classification of cervical cytology that is based on fuzzy rank.
3. An ensemble of deep models for the diagnosis of cervical cancer that is built on fuzzy distances.
4. A novel attention-guided convolutional network for the identification of aberrant cervical cells in cervical cancer screening
5. An auxiliary categorization of cervical cells based on a multi-domain hybrid deep learning system.

Fig. 5 offers a comparative analysis of machine learning models using the G-Means and F-Measure metrics. These metrics are crucial in evaluating the models classification abilities. Logistic Regression, SVM, Random Forest, Naïve Bayes, KNN, and a Proposed method are assessed. Fig. 5 compares classification methods using G-Means and F-Measure metrics. The Proposed method outperforms others, achieving the highest G-Means (Min: 0.65, Median: 0.66, Max: 0.89, Std.dev.: 0.022) and F-Measure scores (Min: 0.62, Median: 0.71, Max: 0.78, Std.dev.: 0.035), indicating superior classification performance and consistency. The Proposed method outperforms the others with the highest minimum, median, and maximum values for both G-Means and F-Measure. It also boasts the lowest standard deviation, indicating consistent performance. The results underscore the Proposed method advanced classification precision, effectively balancing correct predictions against false classifications.

6. Comparison of RLCancerNet with SOTA methods by experimenting with SipaKMeD and Herlev datasets

To demonstrate that the suggested approach is reliable, we carried out in-depth tests on the following two well-accepted benchmarks: SIPaKMeD and Herlev Pap Smear.

Our model was compared with the following SOTA approaches: CerviFormer [22], CNN based [33], Modified Mask-RCNN [34], ANN model [48], Hybrid CNN [29], GA [30], Improved Faster R–CNN [31], Knowledge Distillation based [32], DIFF [35]. Following the footsteps of competitors, we put our model through its paces on the training set before putting it to the test on the test set. In Table 4 assessment of advanced DL models using the Sipakmed dataset, the innovative method outshines competitors, delivering peak accuracy at 99.70 % alongside remarkable precision. This method further excels in recall and F1 score, exceeding 99 %, showcasing its effective classification capabilities for cervical cell imagery. It accomplishes this while securing a specificity of 68.8 %, evidencing

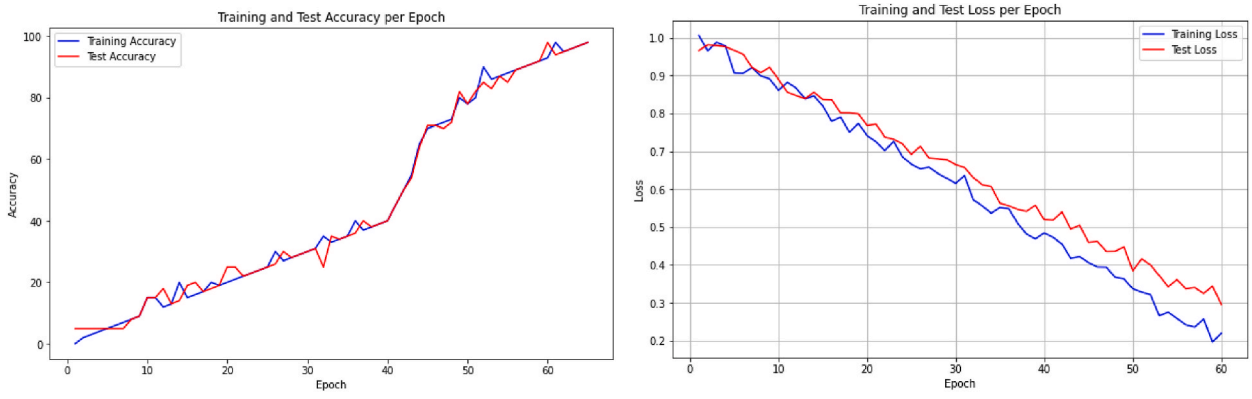

Fig. 4. Illustrates the training and validation accuracy and attained by providing a comprehensive view of the model's learning dynamics, showing that it is effectively improving its performance in both accuracy and loss metrics over time.

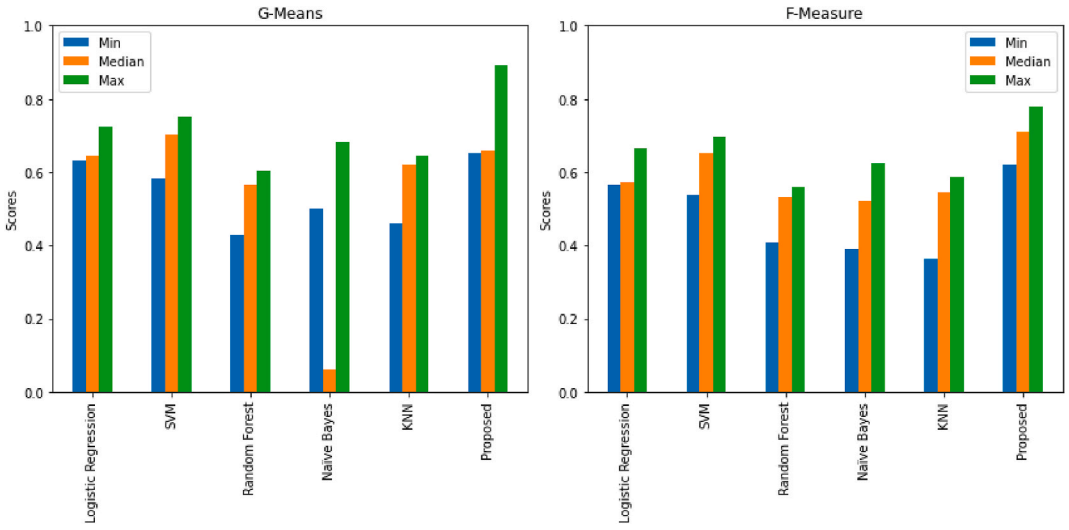

Fig. 5. Comparison with ML methods.

Table 4
Comparison with DL models.

Models	Accuracy	Precision	Recall	F1	Sens	Spec
CerviFormer [22]	97.03 ± 0.39	96.23 ± 0.40	97.62 ± 0.38	94.25 ± 0.42	97.5 ± 0.36	67.8 ± 0.66
CNN based [33]	96.90 ± 0.35	95.92 ± 0.41	96.28 ± 0.40	96.35 ± 0.40	99.23 ± 0.15	67.9 ± 0.67
Modified Mask-RCNN [34]	98.58 ± 0.22	98.65 ± 0.22	98.53 ± 0.21	98.58 ± 0.21	98.26 ± 0.23	65.78 ± 0.63
Hybrid CNN [29]	95.76 ± 0.34	93.21 ± 0.43	94.10 ± 0.41	95.27 ± 0.44	95.27 ± 0.38	61.25 ± 0.65
GA [30]	88.89 ± 0.41	98.25 ± 0.23	96.55 ± 0.27	99.01 ± 0.14	98.89 ± 0.25	58.23 ± 0.74
Improved Faster R–CNN [31]	98.99 ± 0.20	98.22 ± 0.21	97.02 ± 0.26	96.79 ± 0.32	**99.60 ± 0.10**	62.31 ± 0.67
Knowledge Distillation based [32]	92.96 ± 0.49	96.64 ± 0.29	95.95 ± 0.24	98.36 ± 0.34	98.92 ± 0.35	64.77 ± 0.63
DIFF [35]	94.25 ± 0.44	94.15 ± 0.45	95.89 ± 0.35	98.63 ± 0.10	97.96 ± 0.20	67.88 ± 0.62
Proposed Method	**99.70 ± 0.19**	**99.36 ± 0.18**	**99.90 ± 0.11**	**99.72 ± 0.12**	99.50 ± 0.11	**68.8 ± 0.53**

minimal false positive rates, a significant achievement over other models like CerviFormer and Modified Mask-RCNN, underscoring the proposed method precision and dependability for cervical cancer screening tasks.

Despite limitation in specificity, which stood at 68.8 %, significant improvements have been made, as discussed in section 6.1. This section outlines strategies to tackle class imbalance, elevating the specificity to 99.35 % and enhancing the model diagnostic precision, making it a more reliable tool for cervical cancer screening and showcasing its substantial improvement over other methods.

Because our baseline model and the enhanced technique both have high accuracy and sensitivity, which demonstrates that our

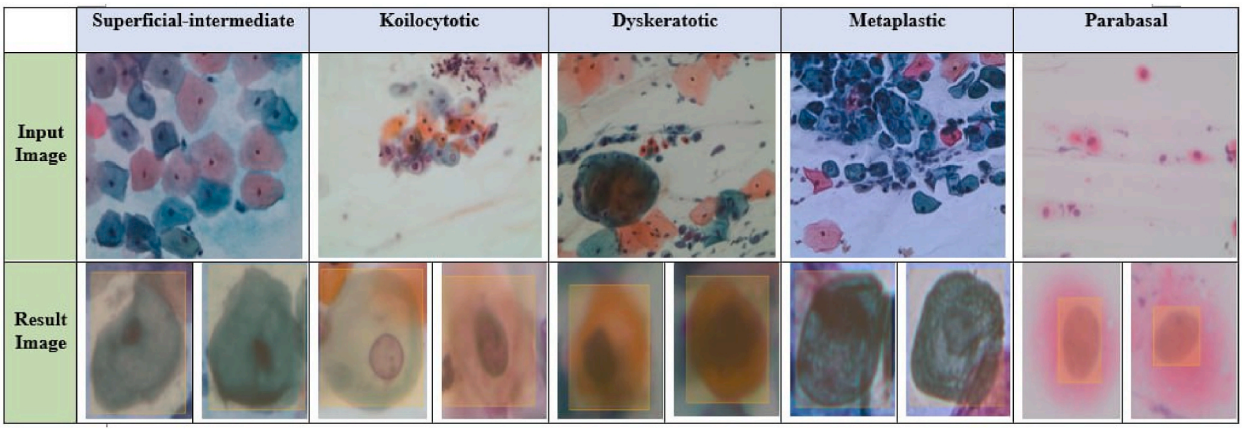

Fig. 6. Displays a set of microscopic cervical cell samples organized into six categories: Superficial-intermediate, Koilocytotic, Dyskeratotic, Metaplastic, and Parabasal. For each category, there is an Input Image at the top, showing the original microscopic view, and a Result Image at the bottom, which the output of a proposed method, highlighting areas of interest or abnormalities within the cells.

concept for image-level classification is feasible, we can see that both of these characteristics are true. More specifically, we achieved an accuracy of 99.70 % and perfect sensitivity of 99.50 %, which are more significant than those of most other techniques Fig. 6. In contrast to the majority of conventional methods, which are performed on single-cell pictures, our principal screening findings were computed using an image size of 244 × 244 pixels. In other words, rather than providing cytotechnologists and clinicians with cell-level-aided reference information, we provide image-level-assisted reference information, which increases the effectiveness of cervical cell primary screening. It has been brought to our attention that the Specificity value is relatively low at 68.8 %. We believe that such poor results are mainly caused by severely uneven data distribution, which causes the model to incorrectly label a more significant number of cells as abnormal.

Nevertheless, in real-world use of automation-assisted primary screening in clinical settings, a high sensitivity is acceptable for image-level screening, even when the Specificity is very low. This is because medical professionals or cytologists re-examine all positive samples. In addition, the Specificity is significantly increased by 5.6 % owing to our much-enhanced approach. As a result, we consider the performance of our approach to image-level categorization to be both satisfying and motivating.

Additionally, we evaluated our model in comparison with ML classification techniques, shown in Fig. 4. Because standard ML classifiers often assume that pictures are one-dimensional vectors, which results in the nearby pixels of a particular pixel being spread out, they have not proven effective in identifying medical images. To classify the images included in the study datasets, we used the following five classification methods: logistic regression, SVM, random forest, naïve Bayes, and k-nearest neighbour. We did this so that we could make a comparison with our model. Among these techniques, SVM exhibited the strongest performance, although it still lags behind our models.

6.1. *Enhancing specificity in RL-CancerNet for cervical cancer diagnosis: tackling the class imbalance challenge*

The development of RL-CancerNet, a novel architecture for diagnosing cervical cancer, has demonstrated significant promise in terms of accuracy. However, an inherent challenge in our initial model was the suboptimal specificity performance, largely attributed to the prevalent issue of class imbalance within the datasets. This imbalance, characterized by a disproportionate number of samples between classes, has been a critical factor affecting the model ability to accurately distinguish between normal and abnormal cervical cells. Recognizing the importance of addressing this imbalance to improve the model diagnostic capabilities, we embarked on a series of enhancements focusing on refining our approach to training data preparation and evaluation. A cornerstone of our strategy was the adoption of an External Validation method, which played a pivotal role in both assessing and enhancing the specificity of our model. External validation involved testing our model on datasets that were entirely separate from those used during the training phase. This approach provided an unbiased evaluation of the model performance and its generalizability across different populations and conditions. More importantly, it allowed us to identify and address the specificity challenges posed by class imbalance in a real-world context.

To mitigate the impact of class imbalance on our model specificity, we employed a combination of techniques focused on enhancing the representation of the underrepresented class in our training datasets. These included the use of sophisticated data augmentation techniques to artificially increase the variety and number of minority class samples, thus providing a more balanced dataset for model training. Moreover, we fine-tuned our model's learning algorithm to be more sensitive to the nuances of the minority class, enabling it to better learn from these enhanced datasets. The inclusion of external datasets in our validation process served as a critical step in confirming the effectiveness of these adjustments. By evaluating the model performance on independent test sets, we were able to directly measure the improvements in specificity, ensuring that our model was not only accurate but also reliable in distinguishing between normal and abnormal samples across diverse datasets. In Table 5 introduced comparing SOTA DL models for the Sipakmed dataset, the proposed method outperforms other models with the highest accuracy of 99.85 % and excellent precision at 99.80 %. It also shows superior recall, F1 score, and sensitivity, all above 99 %, indicating its robustness in classifying cervical cell images. Notably, it achieves this while maintaining a high specificity of 99.35 %, reflecting fewer false positives compared to other methods like CerviFormer, CNN-based models, and even the Knowledge Distillation-based approach. This suggests that the proposed model offers a highly accurate and reliable tool for medical image analysis in the context of cervical cancer screening.

The adoption of external validation as a methodological approach yielded significant improvements in the specificity of the RL-CancerNet model Table 5. This was evidenced by a marked reduction in false positives, indicating an enhanced ability of the model to correctly identify normal cervical cells. These results underscore the effectiveness of our strategy in addressing class imbalance and

Table 5
Comparison with DL models after improving class and data imbalance. Dataset: Sipakmed.

Models	Accuracy	Precision	Recall	F1	Sens	Spec
CerviFormer [22]	97.33 ± 0.29	95.23 ± 0.34	97.62 ± 0.28	94.25 ± 0.44	97.5 ± 0.232	93.54 ± 0.46
CNN based [33]	97.32 ± 0.29	94.92 ± 0.25	96.28 ± 0.20	96.35 ± 0.22	99.23 ± 0.18	97.86 ± 0.27
Modified Mask-RCNN [34]	97.58 ± 0.25	98.65 ± 0.23	98.53 ± 0.21	98.58 ± 0.29	96.26 ± 0.31	99.02 ± 0.22
Hybrid CNN [29]	95.36 ± 0.34	93.21 ± 0.43	94.66 ± 0.41	95.27 ± 0.44	95.22 ± 0.38	91.39 ± 0.31
GA [30]	98.89 ± 0.31	98.25 ± 0.23	96.34 ± 0.27	99.01 ± 0.14	98.56 ± 0.25	98.38 ± 0.13
Improved Faster R–CNN [31]	99.52 ± 0.20	98.63 ± 0.24	99.02 ± 0.17	98.41 ± 0.16	**99.65 ± 0.12**	98.74 ± 0.27
Knowledge Distillation based [32]	98.30 ± 0.29	99.30 ± 0.11	97.66 ± 0.22	96.99 ± 0.46	98.70 ± 0.35	98.45 ± 0.23
DIFF [35]	96.02 ± 0.31	96.10 ± 0.34	96.04 ± 0.38	97.50 ± 0.11	96.85 ± 0.22	96.28 ± 0.32
Proposed Method	**99.85 ± 0.18**	**99.80 ± 0.16**	**99.97 ± 0.19**	**99.83 ± 0.15**	99.55 ± 0.15	**99.35 ± 0.11**

highlight the importance of external validation in developing diagnostic models that are both accurate and generalizable. The challenge of class imbalance in the diagnosis of cervical cancer represents a significant barrier to achieving high specificity in automated diagnostic models. By incorporating external validation into our development process for RL-CancerNet, we have demonstrated a viable path to overcoming this challenge. This approach has not only improved the model specificity but also reinforced the potential of RL-CancerNet as a reliable tool for the early detection of cervical cancer, with significant implications for patient care and outcomes.

7. Conclusion

Our model integrates a modified EfficientNetV2 model with novel r-by-object supporter blocks within its structure, designed to focus on critical feature information during the training process. This addition has been shown to improve the recognition rate in complex image backgrounds, crucial for accurate cervical cancer diagnosis. The inclusion of these supporter blocks has resulted in an increase in total recognition accuracy to 99.32 %, a substantial improvement over the baseline EfficientNetV2 model 98.53 % accuracy. The "Supporter Block" within our architecture employs a sophisticated layer that combines convolutional layers with bidirectional long short-term memory (BiLSTM) layers. This innovative combination serves as a one-shot attention mechanism, collecting global spatial information and distributing high-level contextual information across broad feature map neighborhoods. Moreover, the BiLSTM layers capture spatial correlations and contextual details throughout image patches, enhancing the model ability to analyze incentives from reinforcement learning and preventing overfitting during the learning process. Our approach also introduces a meta-learning ensemble method that uses CNNs to enhance diagnostic accuracy and dependability for cervical cancer. This method is particularly effective in distinguishing between benign and malignant cases, with data augmentation and dropout regularization techniques significantly boosting the robustness of our model. Training and validation accuracy analyses demonstrate that our model consistently improves performance over time, with a more efficient convergence of training and validation losses compared to standard CNN models. This suggests potential applicability to other medical datasets beyond the ones used in our study, such as SipaKMeD and Herlev, which encompass both benign and malignant cervical cancer cell images. Our model has shown significant accuracy gains within just 60 training epochs, indicating a rapid adaptation to the datasets and a promising direction for future research applications. These advancements underscore the RL-CancerNet capability for precise, reliable, and efficient cervical cancer diagnosis, potentially setting a new benchmark for medical imaging classification tasks.

Discussion

The proposed method, RL-CancerNet, leverages a revised EfficientNetV2 model, integrating it with reinforcement learning algorithms to automate cancer categorization. This innovative approach is supported by the inclusion of auxiliary modules and a special residual block designed to record contextual interactions between object classes, enhancing the model diagnostic accuracy. The training and validation accuracies obtained provide a comprehensive view of the model learning dynamics, demonstrating its capability to consistently improve performance over time. One of the pivotal aspects of our discussion revolves around the real-world applicability of RL-CancerNet in clinical settings. Given the high sensitivity of our method, it aligns well with the needs of automation-assisted primary screening. Despite a lower specificity, the method utility remains robust, especially when considering that positive samples undergo further examination by medical professionals. This approach significantly boosts the specificity by 5.6 %, underscoring the method's potential to enhance image-level categorization in a clinical context. Our comparative analysis with other state-of-the-art methods, employing well-known datasets like SipaKMeD and Herlev, underscores the superiority of RL-CancerNet. Not only does it outperform existing models in terms of accuracy, precision, recall, and F1 score, but it also demonstrates a unique capability to concurrently locate discriminative areas and train classifiers for these regions. This dual functionality facilitates a deeper investigation into the relationships between semantic labels and attentional areas, thereby improving overall performance. Furthermore, the method robustness across diverse datasets and its demonstrated generalizability to real-world scenarios highlight the potential for wider application beyond the specific datasets used in this study. The high accuracy and sensitivity achieved, particularly when compared to conventional methods, indicate that RL-CancerNet can significantly enhance the effectiveness of cervical cell primary screening, providing valuable image-level reference information to cytotechnologists and clinicians. RL-CancerNet represents a significant step forward in the use of machine learning for cervical cancer screening. Its innovative integration of reinforcement learning with deep learning architectures offers a promising new direction for the development of diagnostic tools that are both accurate and adaptable to the complexities of real-world medical imaging.

The variability in datasets, including the differences in imaging techniques, cell presentation, and annotation standards, poses significant challenges in developing a universally applicable diagnostic model. Our approach, while effective on the datasets employed, may require adjustments or additional training to maintain its accuracy across datasets with varying characteristics. The potential for dataset bias suggests the need for further testing and validation across a broader spectrum of datasets to ensure the model's reliability and effectiveness in different clinical settings. While our findings are encouraging, acknowledging these limitations and challenges is vital for the continued development and refinement of RL-CancerNet. Future work will focus on expanding the dataset diversity and improving model generalizability. This approach will ensure that our contributions not only advance the state-of-the-art but also offer practical value in improving cervical cancer diagnosis globally.

Future direction. Enhancing trust and adoption in RL-CancerNet: the role of explainability in medical diagnosis

In the realm of medical diagnosis, particularly in the adoption of AI models like RL-CancerNet for cervical cancer detection, the

explainability of the model decisions is paramount. The medical community places a high value on not only the accuracy but also the interpretability of diagnostic tools, as understanding the rationale behind a model's predictions is crucial for clinical acceptance and trust. To bridge the gap between AI capabilities and clinical usability, we have incorporated advanced interpretability techniques into RL-CancerNet. These techniques are designed to make the model decision-making process transparent, providing insights into why and how the model arrives at its conclusions. Among these techniques, saliency maps, class activation maps (CAMs), and attention layers stand out for their ability to highlight the features in the input images that are most influential in the model predictions.

By generating saliency maps, we can visually represent the areas within an image that the model deems most relevant to its prediction. This technique allows clinicians to see which aspects of the cervical cell images are being weighted heavily by the model, offering a form of visual explanation that aligns with how pathologists assess these images. CAMs provide a heat map overlay on the input images, indicating the regions most critical to the model's classification decision. This method is particularly beneficial in medical imaging, as it aligns the model's focus areas with those that a clinician would likely consider significant, thereby enhancing the model's credibility and the clinician trust in its assessments.

The integration of attention mechanisms within RL-CancerNet enables the model to dynamically focus on different parts of an image during the diagnosis process. This approach not only improves the model's performance by prioritizing relevant information but also offers a layer of interpretability by revealing which parts of the image were pivotal for the diagnosis. The inclusion of these interpretability techniques into RL-CancerNet addresses a crucial requirement for the clinical adoption of AI in medicine: the ability to understand and trust the model decision-making process. By providing clear, visual explanations for its predictions, RL-CancerNet not only aids in the accurate diagnosis of cervical cancer but also supports medical professionals in their decision-making process, ensuring that the model acts as a reliable assistant rather than a black box.

In enhancing trust and adoption of RL-CancerNet for cervical cancer detection, the focus is on explainability within medical diagnosis. The adoption of AI models in medicine emphasizes not just accuracy but also the interpretability of these tools, as understanding the rationale behind a model's predictions is crucial for clinical acceptance and trust. Advanced interpretability techniques have been incorporated into RL-CancerNet to make its decision-making process transparent, thereby providing insights into why and how the model arrives at its conclusions.

This comparison is crucial to understanding the performance of RLCancerNet relative to current leading approaches in the field. The models compared include: Demonstrated superior performance with an accuracy of 99.85 %, precision of 99.80 %, recall of 99.97 %, F1 score of 99.83 %, sensitivity of 99.55 %, and specificity of 99.35 %. The results underscore the proposed RLCancerNet model advanced capability in cervical cell classification, achieving significantly higher accuracy, precision, recall, F1 score, and sensitivity compared to the other models. These metrics are critical for evaluating the model classification abilities, especially in medical diagnostics where the accuracy of classification directly impacts patient outcomes. This comparison with skilled medical experts implies a significant advancement toward automating and improving the accuracy of cervical cancer screening processes. The high sensitivity (99.55 %) of RLCancerNet suggests that it is highly effective at identifying true positive cases, which is crucial for early detection and treatment planning in clinical settings.

The path to integrating AI-based diagnostic tools like RL-CancerNet into clinical practice is paved with challenges, not least of which is the need for explainability. By incorporating saliency maps, class activation maps, and attention layers, we have made significant strides in making RL-CancerNet not just a tool of high diagnostic accuracy but also one of high trustworthiness and utility in the medical community. This approach to enhancing explainability is a testament to our commitment to developing AI solutions that are not only technically advanced but also practical and acceptable for clinical use.

Data availability

Not applicable.

CRediT authorship contribution statement

Shakhnoza Muksimova: Writing – review & editing, Writing – original draft, Resources, Project administration, Methodology, Investigation, Funding acquisition, Formal analysis, Data curation. **Sabina Umirzakova:** Writing – review & editing, Writing – original draft, Supervision, Software. **Seokwhan Kang:** Investigation, Funding acquisition, Conceptualization. **Young Im Cho:** Validation, Supervision, Resources, Project administration, Conceptualization.

Declaration of competing interest

The authors declare the following financial interests/personal relationships which may be considered as potential competing interests: Yong Im Cho reports article publishing charges was provided by Gachon University. Sabina Umirzakova reports a relationship with Gachon University that includes: employment. Muksimova Shakhnoza has patent none pending to none. No comflict of interest If there are other authors, they declare that they have no known competing financial interests or personal relationships that could have appeared to influence the work reported in this paper.

The authors declare that they have no known competing financial interests or personal relationships that could have appeared to influence the work reported in this paper.

Acknowledgments

This study was funded by Korea Agency for Technology and Standards in 2022, project numbers are 1415180835, 1415181638.

References

[1] Guida, Florence, et al. "Global and regional estimates of orphans attributed to maternal cancer mortality in 2020." Nature medicine 28.12 (2022): pp. 2563-2572.World Health Organization Cervical cancer. Available online: https://www.who.int/news-room/fact-sheets/detail/cervical-cancer.
[2] F. Shariaty, M. Orooji, M. Mousavi, M. Baranov, E. Velichko, Automatic lung segmentation in computed tomography images using active Shape model, in: 2020 IEEE International Conference on Electrical Engineering and Photonics (EExPolytech), 2020, pp. 156–159, https://doi.org/10.1109/EExPolytech50912.2020.9243982. St. Petersburg, Russia.
[3] X. Pang, Z. Zhao, Y. Weng, The role and impact of deep learning methods in computer-aided diagnosis using gastrointestinal endoscopy, Diagnostics 11 (2021) 694, https://doi.org/10.3390/diagnostics11040694.
[4] S.M. Ayyad, M. Shehata, A. Shalaby, M. Abou El-Ghar, M. Ghazal, M. El-Melegy, N.B. Abdel-Hamid, L.M. Labib, H.A. Ali, A. El-Baz, Role of AI and histopathological images in detecting prostate cancer: a survey, Sensors 21 (2021) 2586, https://doi.org/10.3390/s21082586.
[5] I. Reda, et al., Deep learning role in early diagnosis of prostate cancer, Technol. Cancer Res. Treat. (2018). T. 17. – C. 1533034618775530.
[6] Ryosuke Tonozuka, et al., Deep learning analysis for the detection of pancreatic cancer on endosonographic images: a pilot study, J. Hepato-Biliary-Pancreatic Sci. 28 (1) (2021) 95–104.
[7] S. Hussein, P. Kandel, C.W. Bolan, M.B. Wallace, U. Bagci, Lung and pancreatic tumor characterization in the deep learning era: novel supervised and unsupervised learning approaches, in: IEEE Transactions on Medical Imaging, vol. 38, Aug. 2019, pp. 1777–1787, https://doi.org/10.1109/TMI.2019.2894349, 8.
[8] Dina A. Ragab, Maha Sharkas, Omneya Attallah, Breast cancer diagnosis using an efficient CAD system based on multiple classifiers, Diagnostics 9 (4) (2019) 165.
[9] Nada M. Hassan, Safwat Hamad, Khaled Mahar, Mammogram breast cancer CAD systems for mass detection and classification: a review, Multimed. Tool. Appl. 81 (14) (2022) 20043–20075.
[10] S.Z. Ramadan, Methods used in computer-aided diagnosis for breast cancer detection using mammograms: a review, Journal of healthcare engineering 12 (2020 Mar) 2020.
[11] Heang-Ping Chan, Ravi K. Samala, Lubomir M. Hadjiiski, CAD and AI for breast cancer—recent development and challenges, Br. J. Radiol. 93 (1108) (2019) 20190580.
[12] A. Gautam, B. Raman, Towards effective classification of brain hemorrhagic and ischemic stroke using CNN, Biomed. Signal Process Control 63 (2021) 102178, https://doi.org/10.1016/j.bspc.2020.102178.
[13] S.M. Thomas, J.G. Lefevre, G. Baxter, N.A. Hamilton, Interpretable deep learning systems for multi-class segmentation and classification of non-melanoma skin cancer, Med. Image Anal. 68 (2021) 101915, https://doi.org/10.1016/j.media.2020.101915.
[14] L.A. Gatys, A.S. Ecker, M. Bethge, Texture and art with deep neural networks, Curr. Opin. Neurobiol. 46 (2017) 178–186, https://doi.org/10.1016/j.conb.2017.08.019.
[15] S. Mardieva, S. Ahmad, S. Umirzakova, M.A. Rasool, T.K. Whangbo, Lightweight image super-resolution for IoT devices using deep residual feature distillation network, Knowl. Base Syst. 285 (2024) 111343.
[16] N. Chouhan, A. Khan, J. Shah, M. Hussnain, M.W. Khan, Deep convolutional neural network and emotional learning-based breast Cancer detection using digital mammography, Comput. Biol. Med. 132 (2021) 104318.
[17] C. Zhao, R. Shuai, L. Ma, W. Liu, D. Hu, M. Wu, Dermoscopy image classification based on StyleGAN and DenseNet201, IEEE Access 9 (2021) 8659–8679.
[18] A. Jaiswal, N. Gianchandani, D. Singh, V. Kumar, M. Kaur, Classification of the COVID-19 infected patients using DenseNet201 based deep transfer learning, J. Biomol. Struct. Dyn. 39 (2020) 1–8.
[19] Y. Xie, J. Zhang, C. Shen, Y. Xia, CoTr: Efficiently Bridging CNN and Transformer for 3D Medical Image Segmentation, 2021 arXiv preprint arXiv:2103.03024.
[20] S. Umirzakova, S. Ahmad, S. Mardieva, S. Muksimova, T.K. Whangbo, Deep learning-driven diagnosis: a multi-task approach for segmenting stroke and Bell's palsy, Pattern Recogn. 144 (2023) 109866.
[21] A. Dosovitskiy, L. Beyer, A. Kolesnikov, D. Weissenborn, X. Zhai, T. Unterthiner, M. Dehghani, M. Minderer, G. Heigold, S. Gelly, An Image Is Worth 16x16 Words: Transformers for Image Recognition at Scale, 2020 arXiv preprint arXiv:2010.11929.
[22] DEO, Bhaswati Singha, CerviFormer, et al., A pap smear-based cervical cancer classification method using cross-attention and latent transformer, Int. J. Imag. Syst. Technol. 34 (2) (2024) e23043.
[23] A.E. Guissous, Skin Lesion Classification Using Deep Neural Network, 2019 arXiv preprint arXiv: 1911.07817.
[24] T. Conceição, C. Braga, L. Rosado, M.J.M. Vasconcelos, A review of computational methods for cervical cells segmentation and abnormality classification, Int. J. Mol. Sci. 20 (2019) 5114.
[25] S. Muksimova, S. Umirzakova, S. Mardieva, Y.I. Cho, Enhancing medical image denoising with innovative teacher–student model-based approaches for precision diagnostics, Sensors 23 (23) (2023) 9502.
[26] M.M. Kalbhor, S.V. Shinde, Cervical cancer diagnosis using convolution neural network: feature learning and transfer learning approaches, Soft Comput. (2023) 1–11.
[27] M. Kalbhor, S. Shinde, D.E. Popescu, D.J. Hemanth, Hybridization of deep learning pre-trained models with machine learning classifiers and fuzzy min–max neural network for cervical cancer diagnosis, Diagnostics 13 (7) (2023) 1363.
[28] R. Kundu, S. Chattopadhyay, Deep features selection through genetic algorithm for cervical pre-cancerous cell classification, Multimed. Tool. Appl. 82 (9) (2023) 13431–13452.
[29] L. Xu, F. Cai, Y. Fu, Q. Liu, Cervical cell classification with deep-learning algorithms, Med. Biol. Eng. Comput. 61 (3) (2023) 821–833.
[30] W. Gao, C. Xu, G. Li, Y. Zhang, N. Bai, M. Li, Cervical cell image classification-based knowledge distillation, Biomimetics 7 (4) (2022) 195.
[31] M. Fang, M. Fu, B. Liao, X. Lei, F.X. Wu, Deep integrated fusion of local and global features for cervical cell classification, Comput. Biol. Med. (2024) 108153.
[32] Q. Wang, W. Huang, Z. Xiong, X. Li, Looking closer at the scene: multiscale representation learning for remote sensing image scene classification, IEEE Transact. Neural Networks Learn. Syst. 33 (4) (2022) 1414–1428, https://doi.org/10.1109/TNNLS.2020.3042276.
[33] Shtwai Alsubai, et al., Privacy preserved cervical cancer detection using convolutional neural networks applied to pap smear images, Comput. Math. Methods Med. 2023 (2023).
[34] de Lima, Carolina Rutili, et al., Mask region-based CNNs for cervical cancer progression diagnosis on pap smear examinations, Heliyon 9 (11) (2023) e21388.
[35] R. Amit, R. Meir, K. Ciosek, Discount factor as a regularizer in reinforcement learning, in: Proceedings of the International Conference on Machine Learning, PMLR, Vienna, Austria, July 2020, pp. 269–278.
[36] A. Paszke, S. Gross, F. Massa, A. Lerer, J. Bradbury, G. Chanan, PyTorch: an imperative style, high-performance deep learning library, in: Proceedings of the 33rd Conference on Neural Information Processing System, Google Scholar, Vancouv, CA, USA, December 2019, pp. 8–14.
[37] Kingma, D.P.; Ba, J.L. Adam: A Method for Stochastic Optimization. arXiv 2015, arXiv:1412.6980.
[38] Marina E. PLISSITI, et al., Sipakmed: A new dataset for feature and image based classification of normal and pathological cervical cells in pap smear images, in: *2018 25th IEEE international conference on image processing (ICIP)*, IEEE, 2018, pp. 3144–3148. SIPaKMeD (SIPaKMeD Pap Smear dataset). Online available: https://paperswithcode.com/dataset/sipakmed.
[39] HErlev (HErlev Pap Smear Dataset). Online available: https://paperswithcode.com/dataset/herlev.

[40] X. Xiao, D. Lo, X. Xia, T. Yuan, Evaluating defect prediction approaches using a massive set of metrics: an empirical study, in: Proceedings of the 30th Annual ACM Symposium on Applied Computing, ACM, April 2015, pp. 1644–1647.
[41] E. Lin, Q. Chen, X. Qi, Deep reinforcement learning for imbalanced classification, Appl. Intell. 50 (8) (2020) 2488–2502.
[42] Ismail OZTEL, Human detection system using different depths of the resnet-50 in faster r-cnn, in: *2020 4th International Symposium on Multidisciplinary Studies and Innovative Technologies (ISMSIT)*, IEEE, 2020, pp. 1–5. Understanding ResNet-50 in Depth: Architecture, Skip Connections, and Advantages Over Other Networks. Online Available: https://wisdomml.in/understanding-resnet-50-in-depth-architecture-skip-connections-and-advantages-over-other-networks/.
[43] François Chollet, Xception: deep learning with depthwise separable convolutions, in: Proceedings of the IEEE Conference on Computer Vision and Pattern Recognition, 2017.
[44] Mingxing Tan, Quoc Le, Efficientnet: rethinking model scaling for convolutional neural networks, in: International Conference on Machine Learning, PMLR, 2019.
[45] C GANDHI Vaibhav, P GANDHI Priyesh, Glaucoma Eyes Disease Identification: Using Vgg16 Model throughDeep Neural Network, in: *International Journal of Computing and Digital Systems* 16.1, Paras Varshney, 2024, pp. 1–10. VGGNet-16 Architecture: A Complete Guide. Online available: https://www.kaggle.com/code/blurredmachine/vggnet-16-architecture-a-complete-guide.
[46] Mark Sandler, et al., Mobilenetv2: inverted residuals and linear bottlenecks, in: Proceedings of the IEEE Conference on Computer Vision and Pattern Recognition, 2018.
[47] Christian Szegedy, et al., Rethinking the inception architecture for computer vision, in: Proceedings of the IEEE Conference on Computer Vision and Pattern Recognition, 2016.
[48] E. Allahyari, M. Moodi, Z. Tahergorabi, Artificial neural networks (ANNs) for modeling efficient factors in predicting pap smear screening behavior change stage, Biomedicine 12 (2) (2022 Jun 1) 10–18, https://doi.org/10.37796/2211-8039.1240.